International Journal of Minerals, Metallurgy and Materials
Volume 28, Number 12, December 2021, Page 1875
https://doi.org/10.1007/s12613-020-2237-3

Mechanical properties and energy evolution of jointed rock specimens containing an opening under uniaxial loading

Peng Li[1,2,3], *Mei-feng Cai*[1,2,3], *Pei-tao Wang*[1,2,3], *Qi-feng Guo*[1,2,3], *Sheng-jun Miao*[1,2,3], *and Fen-hua Ren*[1,2,3]

1) School of Civil and Resource Engineering, University of Science and Technology Beijing, Beijing 100083, China
2) Key Laboratory of High-Efficient Mining and Safety of Metal Mines (Ministry of Education of China), University of Science and Technology Beijing, Beijing 100083, China
3) Beijing Key Laboratory of Urban Underground Space Engineering, University of Science and Technology Beijing, Beijing 100083, China
(Received: 5 September 2020; revised: 2 December 2020; accepted: 8 December 2020)

Abstract: To investigate the impact of an opening and joints with different inclination angles on the mechanical response behavior, the energy evolution characteristics, and distribution law of granite specimens, uniaxial loading tests were performed on the parallel jointed rock samples with an opening. Results indicated an initial decreasing trend of the strength and deformation parameters, which later increases with increased inclination angle, reaching minimum values when the inclination angle is 45°. Evolution curves of the elastic strain energy and dissipated energy with strain of the samples showed step-like gradual mutation characteristics. The peak total energy, peak elastic strain energy, peak dissipated energy, and total input energy during the failure of the samples showed significant nonlinear characteristics with increasing inclination angle. The opening and joints as well as the change of the inclination angle had significant influences on the proportion of the elastic strain energy of the samples prior to the peak, resulting in the difference of the distribution law of input energy. Moreover, the energy mechanism of the sample failure was discussed. Results showed that the energy release was the internal cause of the sudden destruction of the entire rock mass.

Keywords: rock mechanics; mechanical properties; energy evolution; jointed rock specimens containing an opening; uniaxial loading

1. Introduction

Rock masses are typically natural geological materials exhibiting nonlinearity, discontinuity, heterogeneity, and anisotropy. After a long geological process, discontinuous structural planes such as joints, fissures, weak interlayers, holes, and faults, with different geometries and scales, are randomly distributed in the rock mass. During rock mass failure, these discontinuities have a considerable influence on the mechanical response, showing strong nonlinear characteristics. As a result, evaluation of the deformation and failure features of the rock mass in most underground engineering, such as mining engineering, is difficult. However, rock deformation is essentially irreversible due to the energy transformation and transfer, and the final failure indicates an instability state with the internal energy as the driving force [1–2]. The damage evolution process of the loaded rock is bounded by the energy conversion mechanism, and the rock demonstrates discrepant energy conversion features in each loading stage. Hence, studying the law of engineering rock mass deformation and failure from the perspective of energy evolution is closer to the nature of rock mass failure, which can provide a new perspective and scheme for solving rock mechanics problems such as rock bursts, roof caving, and large deformation of roadway surrounding rock.

Numerous theoretical and experimental surveys have been performed to observe the mechanical properties of rocks and the law of energy transformation and transmission during the loaded rock deformation and failure. A lot of valuable achievements have been derived. For instance, Xie *et al.* [3] studied the rock deformation and failure from the energy point and explained the energy dissipation and release features in this process. Zhang *et al.* [4] established a self-restraint evolution model of energy transformation with axial stress by analyzing the nonlinear relation among discrepant energy transformation mechanisms and observed the law of energy evolution in dry and wet red sandstone. Zuo *et al.* [5] studied the entire process of deformation and failure in brittle

Corresponding author: Fen-hua Ren E-mail: renfh_2001@163.com

rocks and proposed to use the energy drop coefficient to characterize the parameters of rock failure. Li *et al.* [6] investigated the whole transformation process and energy evolution mechanism among the total absorbed energy, elastic strain energy, and dissipated energy of shale. Gong *et al.* [7] studied the evolution law of different types of energy during rock tensile failure using various test methods. Liu *et al.* [8] discussed the influence of saturation on strength parameters, deformation characteristics, and energy evolution of Badong formation mudstone, and then established the internal relationship among mechanical properties, energy evolution, and microcrack development. Meng *et al.* [9] characterized the energy accumulation, dissipation, and release behavior of loaded rocks using characteristic energy density and energy consumption ratio parameters. Chen *et al.* [10] comprehensively considered the accumulation characteristics of elastic strain energy before the peak point and its release features after the peak point and established an evaluation index of rock brittleness according to the entire process of elastic strain energy evolution.

Previous researches have vigorously prompted the progress of rock energy theory in rock mechanics and enriched and deepened the cognition of the mechanical response of loaded rocks. However, existing research results mainly focus on the energy evolution law of loaded intact rocks, while less emphasis has been placed on the energy evolution law of jointed rock mass, especially those containing an opening under loading, which is exactly the key to the failure mechanism analysis and stability control of the surrounding rocks of underground engineering caverns. Therefore, the energy mechanism of strength weakening of the jointed rock mass with an opening needs to be further studied. To that end, the uniaxial compression tests are performed in the present article to study the energy evolution law of intact rock specimens, intact rock specimens containing an opening, and jointed rock specimens containing an opening in the process of deformation and failure. The analysis is done on the influence of the opening and joints with different angles on the total energy, elastic strain energy, and dissipated energy. Moreover, the action law of these factors on the energy storage capacity, energy dissipation mechanism, and damage and failure evolution mechanism of those samples is revealed. The research results are of great theoretical value and engineering significance for further understanding the damage and energy evolution mechanism of jointed rock masses and improving the energy theory system of rock mechanics.

2. Experimental

2.1. Specimen preparation and material properties

The granite samples used in the experiments are all sourced from the Laizhou area, Shandong Province, China. The tested granite was dense in texture without visible defects and was mainly composed of plagioclase, quartz, and biotite. The intact cuboid granite samples were first processed by the mechanical cutting method. During the machining process, all samples were cut in the same orientation to avoid the impact of anisotropy on the results of the test. Hence, identical, intact, and undisturbed granite samples with a nominal size of 100 mm × 35 mm × 35 mm (length × width × thickness) were processed (Fig. 1(a)). The length-to-width ratio of the tested samples was about 2.86, which conformed to the testing standard of the uniaxial loading test recommended by the International Society for Rock Mechanics (ISRM), which is a length-to-width ratio of 2.5–3.0 [11]. Consequently, all specimens with a length-to-width ratio of 2.86 guarantee that the central part of the specimens is in a uniform stress state.

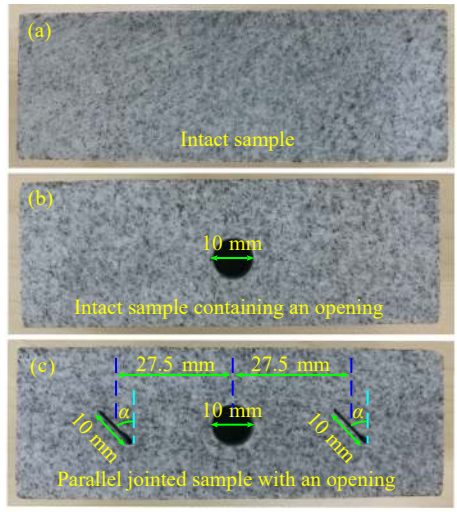

Fig. 1. Photos of different granite samples: (a) intact granite sample; (b) intact samples containing an opening; (c) parallel jointed samples with an opening.

After the intact samples were prepared, circular openings and parallel joints were produced using an improved high-pressure water jet cutting equipment. A circular hole of 10 mm in diameter was created in the central part of the intact samples, which was called the intact sample containing an opening (Fig. 1(b)). Further, two parallel joints with varying inclination angles α (α = 0°, 15°, 30°, 45°, 60°, 75°, and 90°) and symmetrically distributed with the circular opening as the center were produced through the intact samples containing an opening, which was regarded as the parallel jointed samples with an opening (Fig. 1(c)). For all parallel jointed samples with an opening, the geometric dimensions of the two parallel joints were the same, and the joints were approximately 10 mm long and 0.8 mm wide. To obtain reliable and accurate test results, all tested specimens had been polished to guarantee parallelism and perpendicularity of the loading surfaces and smoothness of the opening and joint surfaces [12]. The nonlinearity and non-perpendicularity of the end

faces of the specimens were controlled to be smaller than 0.02 mm, which meet the basic requirements of the rock mechanics test and minimize the influence of the end friction effect during loading [13].

The prepared samples were divided into several groups and named according to sample type to better distinguish them. Three samples were prepared for each group, which was beneficial in obtaining reliable and convincing test results. In the sample number, UI stands for the intact samples, UC denotes the intact samples containing an opening, and the digits followed by them represent the test serial numbers of the samples. UCJ stands for the parallel jointed samples with an opening, where the first and second digits behind it represent the inclination angle of the joint and the test serial numbers of the samples, respectively. From this point, we use the nomenclatures UI, UC, UCJ to denote the intact samples, intact samples containing an opening, and parallel jointed samples with an opening, respectively.

The common physical and mechanical parameters of the intact granite samples were obtained according to standard rock mechanics test methods suggested by the ISRM [11]. The average unit weight, uniaxial compressive strength, tensile strength, elastic modulus, and Poisson's ratio of the intact granite specimen were 2595 kg/m^3, 251.27 MPa, 17.85 MPa, 34.61 GPa, and 0.21, respectively. Thus, it follows that the granite possesses high strength, and exhibits a uniaxial compressive strength to tensile strength ratio of approximately 14, which suggests that the granite samples belong to a typical brittle or quasi-brittle rock type [14].

2.2. Testing facilities

The uniaxial loading test was performed with a TAW-3000 rock mechanics servo-controlled testing machine. The maximum axial bearing capacity of the test system approaches 3000 kN, and the loads and displacements of the samples during loading can be automatically acquired and recorded by the loading equipment in real time. Moreover, the machine can realize full curve drawing, and has the advantages of various loading modes, stable equipment performance, and high control precision.

2.3. Testing procedures

The prepared sample was put on the test bench. The upper and lower loading ends of the sample are evenly coated with a layer of Vaseline and then pasted with a thin paper of the same cross-section size. After that, two rigid steel blocks were put amid the loading frame and the specimen to minimize the friction effect between the sample and the loading plate during the test. A vertical load of 2 kN was applied in advance to guarantee full contact between the specimen end face and the loading plate. When the loading begins, the vertical load increased gradually until the specimen failure took place. Uniaxial loading tests were performed using the displacement-controlled mode under the constant loading rate of 0.1 mm/min (the corresponding strain rate was about 1.67×10^{-5} s^{-1}). This low loading rate can eliminate the dynamic disturbance of the testing machine on the samples and guarantee the quasi-static balance of the samples during the test [15].

2.4. Energy calculation methods

Generally, the deformation and failure process of loaded rocks is regarded as a closed system, i.e., it is assumed that the rock has no exchange of heat with the outside during the entire loading process. Thus, the energy driven by the external force is determined as

$$U = U_d + U_e \tag{1}$$

where U, U_e, and U_d correspond to the external energy input, elastic strain energy, and the dissipated energy that is in charge of the plastic deformation and cracks propagation of rocks, respectively.

Given the reversibility of the elastic strain energy, U_e and U_d of rocks can be computed with the knowledge of the stress–strain curve under loading and unloading. It is generally believed that the energy released after unloading equates to the elastic strain energy accumulated at the stress level when unloading, and the reduction relative to the total energy under loading equates to the energy dissipated under the stress level. Fig. 2 displays the schematic diagram of the link between U_e and U_d, in which the shaded area suggests the U_e accumulated in rocks because of deformation. The area enclosed by the unloading elastic modulus E_u, stress–strain curve, and the horizontal axis denotes the U_d. In a three-dimensional condition, the energy calculation formula per unit volume of rock is defined as

$$U = \int_0^{\varepsilon_1} \sigma_1 d\varepsilon_1 + \int_0^{\varepsilon_2} \sigma_2 d\varepsilon_2 + \int_0^{\varepsilon_3} \sigma_3 d\varepsilon_3 \tag{2}$$

$$U_e = \frac{1}{2}\sigma_1\varepsilon_{e1} + \frac{1}{2}\sigma_2\varepsilon_{e2} + \frac{1}{2}\sigma_3\varepsilon_{e3} \tag{3}$$

According to Hooke's law, Eq. (3) can be transformed into

$$U_e = \frac{1}{2E_0}\left[\sigma_1^2 + \sigma_2^2 + \sigma_3^2 - 2\nu(\sigma_1\sigma_2 + \sigma_2\sigma_3 + \sigma_1\sigma_3)\right] \tag{4}$$

where σ_i (i = 1, 2, 3) refers to the principal stress; ε_i (i = 1, 2, 3) corresponds to the principal strain, and the lateral strain ε_2 and ε_3 of the rock after compression are negative (the compressive strain is positive); ε_{ei} (i = 1, 2, 3) suggests the corresponding elastic strain; E_0 indicates the elastic modulus; and ν denotes the Poisson's ratio.

To conveniently calculate the releasable U_e per unit volume, the unloading curve and the reloading curve of rocks on the stress–strain curve are usually regarded to be basically consistent, i.e., E_u approximates E_0. When computing U_e, which corresponds to any point of the stress–strain curve, it can be defined pursuant to the stress value and elastic modulus

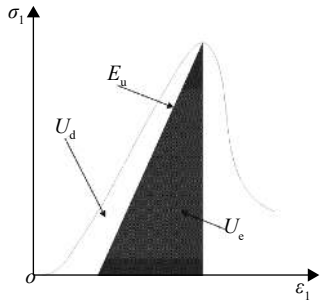

Fig. 2. Relationship between the elastic strain energy and dissipated energy in rock.

of that point. Therefore, for the uniaxial compression, the energy per unit volume of rocks is simplified as below:

$$U = \int_0^{\varepsilon_1} \sigma_1 d\varepsilon_1 \tag{5}$$

$$U_e = \frac{1}{2E_0}\sigma_1^2 \tag{6}$$

U_d is determined as

$$U_d = U - U_e \tag{7}$$

3. Analysis of mechanical properties

3.1. Axial stress–strain relationship

Fig. 3 presents the axial stress–strain curves of the intact sample (UI) and the intact sample containing an opening (UC) subjected to uniaxial loading. Shortly after reaching the peak strength, the stress drops sharply to nearly zero with the huge sound of specimen rupture. The stress–strain curve of the UI is in good accordance with the representative brittle behavior model [16], which indicates that the granite specimen has strong brittle or quasi-brittle failure characteristics. This is further confirmed by the final failure characteristic of UI, which is a typical vertical splitting failure as shown in Fig. 4. On the other hand, UI has an especially smooth stress–strain curve before peak strength, whereas the stress–strain curve of UC exhibits two noticeable stress drops prior to peak strength, which suggests that the existence of opening enhances the plastic properties of the granite specimen.

Fig. 5(a) plots the stress–strain curves for the parallel jointed specimens containing an opening (UCJ) subjected to uniaxial loading. Obviously, each specimen has a highly nonlinear process of deformation and failure, but the stress–strain curves of the samples are quite similar. Moreover, all specimens reveal remarkable elastic-brittle failure features but demonstrate a degree of plastic deformation close to the peak strength.

Taking UCJ-15-3 as an example, the change process on the stress–strain curve (Fig. 5(b)) of the specimen generally consists of five stages: (1) initial compaction stage (*OA*), (2) elastic deformation stage (*AB*), (3) stable crack propagation stage (*BC*), (4) unstable crack propagation stage (*CD*), and (5) residual strength stage (after point *D*). Specifically, the

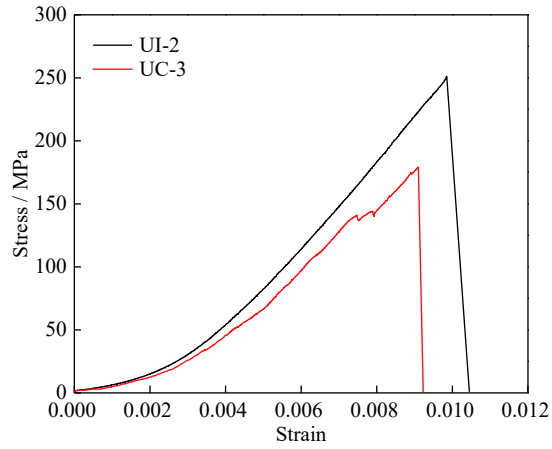

Fig. 3. Axial stress–strain curves of the intact specimen, UI, and the intact sample containing an opening, UC, under uniaxial compression test.

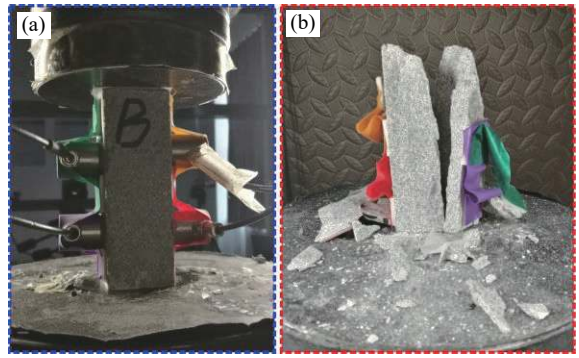

Fig. 4. Failure characteristics of the intact specimen under uniaxial loading: (a) before failure; (b) after failure.

stress–strain curve in the initial compaction stage slightly bends upward and develops nonlinearly (concave), suggesting increasing axial stiffness induced by the compaction of original microscopic or submicroscopic pores/cracks in the specimens. The scope of this stage is primarily determined by the defect population's original defect density and geometric features [17]. The stress–strain curves of the different samples are observed to exhibit little difference. During the stable crack propagation stage, stress concentration begins to appear around the joint tip and/or opening in the specimen, and cracks start to initiate and propagate stably when the stress intensity factor in the local area reaches the critical stress of crack initiation. Moreover, distinct stress drops are observed at the stage of unstable crack propagation, implying rapid crack initiation, propagation, and coalescence in the local area of the samples. After several stress drops, cracks develop rapidly, cross, and penetrate each other to form macroscopic fracture surfaces. The sample will reach its peak strength quickly and brittle failure will appear accompanied by an increase of axial deformation. The bearing capacity of the specimen will then drop sharply. However, some samples are not completely destroyed when the peak strength is

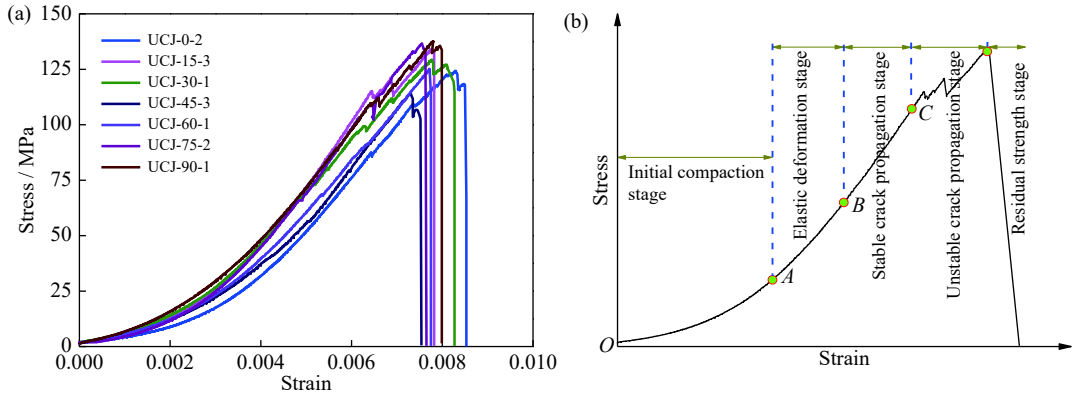

Fig. 5. (a) Stress–strain curves of the parallel jointed samples with an opening and (b) schematic diagram of the stress–strain curve stage division of the sample.

reached, and a short time lag occurs between the peak point and the final failure point, primarily due to the friction of serrated crack surfaces. The strength of the specimen is mainly the residual friction along the fracture surface, and the deformation resistance is very small; hence, the deformation in the residual strength stage is mainly characterized by the shear sliding deformation along the localized zone. Note that the residual strength stage is not remarkable on the stress–strain curves of UI and UC, but it only exists on the stress–strain curves of some parallel jointed samples with an opening.

Comparing the stress–strain curves of the specimens, it can be observed that the presence of the opening and joints in UCJ will change the stress–strain features of rocks partly, i.e., enhance the plastic properties of the granite. Moreover, the stress–strain curves of these samples show a certain fluctuation near the peak strength. For UCJ, the stress–strain curves show multiple stress drops in the case of a small inclination angle (such as 0° and 15°). As inclination angle increases, the times of stress drops of the samples during deformation and failure overall decrease, indicating that the plastic deformation behavior of the samples decreases with increasing inclination angle. Each large crack propagation in the sample corresponds to a large stress drop on the stress–strain curve, and the difference in the shape of the stress–strain curve is also an external manifestation of the different evolution processes of the crack propagation in samples. Therefore, the variation characteristics of the stress–strain curves can indicate whether the rock mass has weak structural planes that can influence its mechanical response.

3.2. Strength and deformation behavior

Fig. 6 illustrates the changes of the peak strength and elastic modulus of UCJ with varying inclination angles, reflecting the effect of the inclination angle on the two mechanical parameters. The intact sample has the largest peak strength, reaching 251.27 MPa, whereas the peak strength of the UC is decreased to 179.27 MPa with a reduction of 28.65% to the UI. This indicates the remarkable impact of the opening on the rock's strength property. As shown in Fig. 6(a), the peak strengths of UCJ with inclination angles of 0°–90° are between 114.65 and 137.67 MPa, showing a reduction of 45.21%–54.37%, compared to UI. The drastic decrease of the peak strength of UCJ indicates that the presence of the opening and joints can significantly weaken the strength property of the granite. This is mainly because the opening and joints reduce the relative size of the specimen,

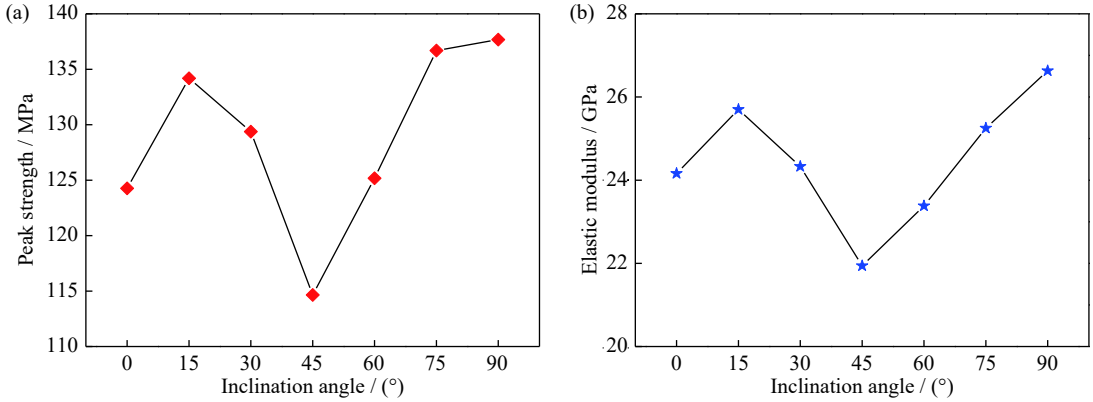

Fig. 6. Influence of inclination angle on the mechanical parameters of the parallel jointed samples containing an opening: (a) peak strength; (b) elastic modulus.

weaken the supporting capacity of the specimen, and intensify the stress concentration around the opening and joint tips, making the specimen more prone to fracture. In addition, the minimum and maximum peak strengths are reached at around 45° and 90°, respectively. Overall, the peak strength shows a nonlinear trend of initially decreasing and then increasing as the inclination angle increases.

The elastic modulus (the mean slope of a straight line on the stress–strain curve) of the UI is highest with a value of 34.61 GPa, whereas the elastic modulus of the UC is 30.58 GPa, showing a reduction of 11.64% compared to UI. Fig. 6(b) depicts the influence of the inclination angle on the elastic modulus of UCJ subjected to uniaxial compression. The elastic moduli of UCJ with inclination angles of 0°–90° are between 21.94 and 26.63 GPa, which are reduced by 23.06%–36.61%, compared to the UI. Additionally, with the increase of inclination angle, the elastic modulus of UCJ varies nonlinearly, i.e., the elastic modulus first decreases and then increases, reaching the minimum and maximum values when the inclination angles are 45° and 90°, respectively. In general, the elastic modulus and the peak strength have a similar change trend. However, the influence degree of the opening and joints on the elastic modulus is noticeably less than that on the peak strength.

In summary, the mechanical performance of granite is degraded by the presence of the opening and joints and is affected by the inclination angle. Moreover, the obtained effective mechanical parameters of the indoor jointed samples appear to better forecast the mechanical performance of engineering rock mass with specific approaches or criteria (such as Hoek-Brown strength criterion), which can provide important parameters for underground engineering construction, stability analysis of chamber surrounding rock, and optimization design of chamber support.

4. Energy evolution analysis

4.1. Energy evolution process and law

According to the above-mentioned energy calculation methods, the evolution process of U, U_e, and U_d of the samples with strain can be obtained under uniaxial loading. Figs. 7–8 show the evolutionary relationship of U, U_e, and U_d with strain for UI (Fig. 7(a)), UC (Fig. 7(b)), and UCJ (Fig. 8). Basically, the energy evolution models of all samples are relatively similar. Both U and U_e show a nonlinear increase as the load increases, in which U_e shows a trend of first increasing and then decreasing. On the other hand, U_d increases quite slowly before specimen failure and increases sharply. Its value suddenly exceeds U_e when the specimen approaches failure.

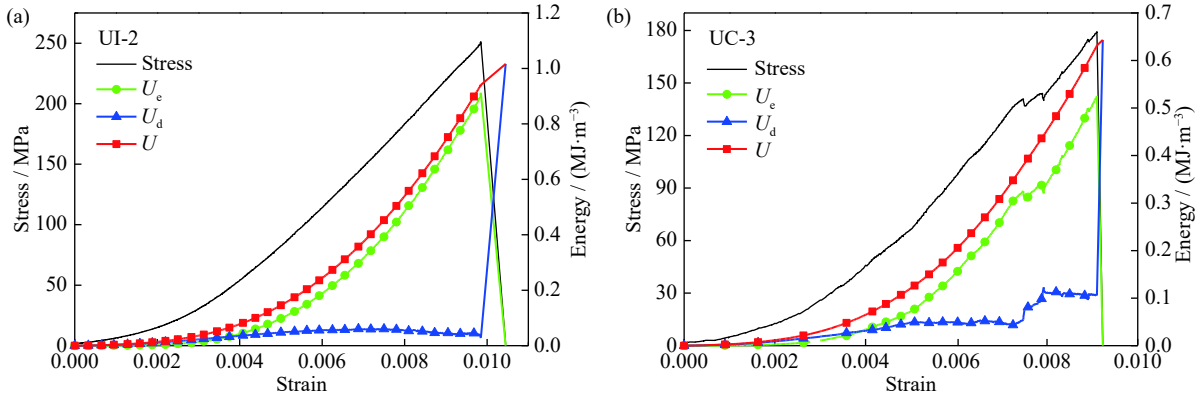

Fig. 7. Stress–strain and energy evolution curves of (a) the intact sample and (b) the intact sample containing an opening.

However, there are some differences in energy evolution characteristics of different samples. In the initial compaction stage, the absorbed U and U_e by all samples increase roughly in a parabolic shape with strain. U_d grows in a flat "S" shape with strain and exhibits a higher growth rate compared with U_e. This phenomenon is more obvious in the energy curves of UC and UCJ because the microcrack closure and friction in the samples will consume most of the energy at this stage, and the self-adaptive adjustment of the opening and joints to the initial load will also consume energy. As the load increases, the microcracks in the specimen gradually close, resulting in the increase of the effective contact area. Moreover, the self-adaptive adjustment of the opening and joints tends to be stable. The growth rate of U_d starts to decrease, while the growth rate of the U_e begins to increase and gradually exceeds that of U_d and is basically the same as that of U. During the elastic deformation stage, U and U_e have a nearly linear growing trend as strain increases, while U_d has a progressive slower growth rate and remains constant. The absorbed energy is mostly transferred into elastic strain energy and stored in samples with very small energy dissipation. In the stable crack propagation stage, one part of the work (total input energy) exerted by external force on the specimen is used to initiate, propagate, and coalesce cracks in samples, while the remaining part is still preserved in the specimens as elastic strain energy. Due to the brittleness of the granite

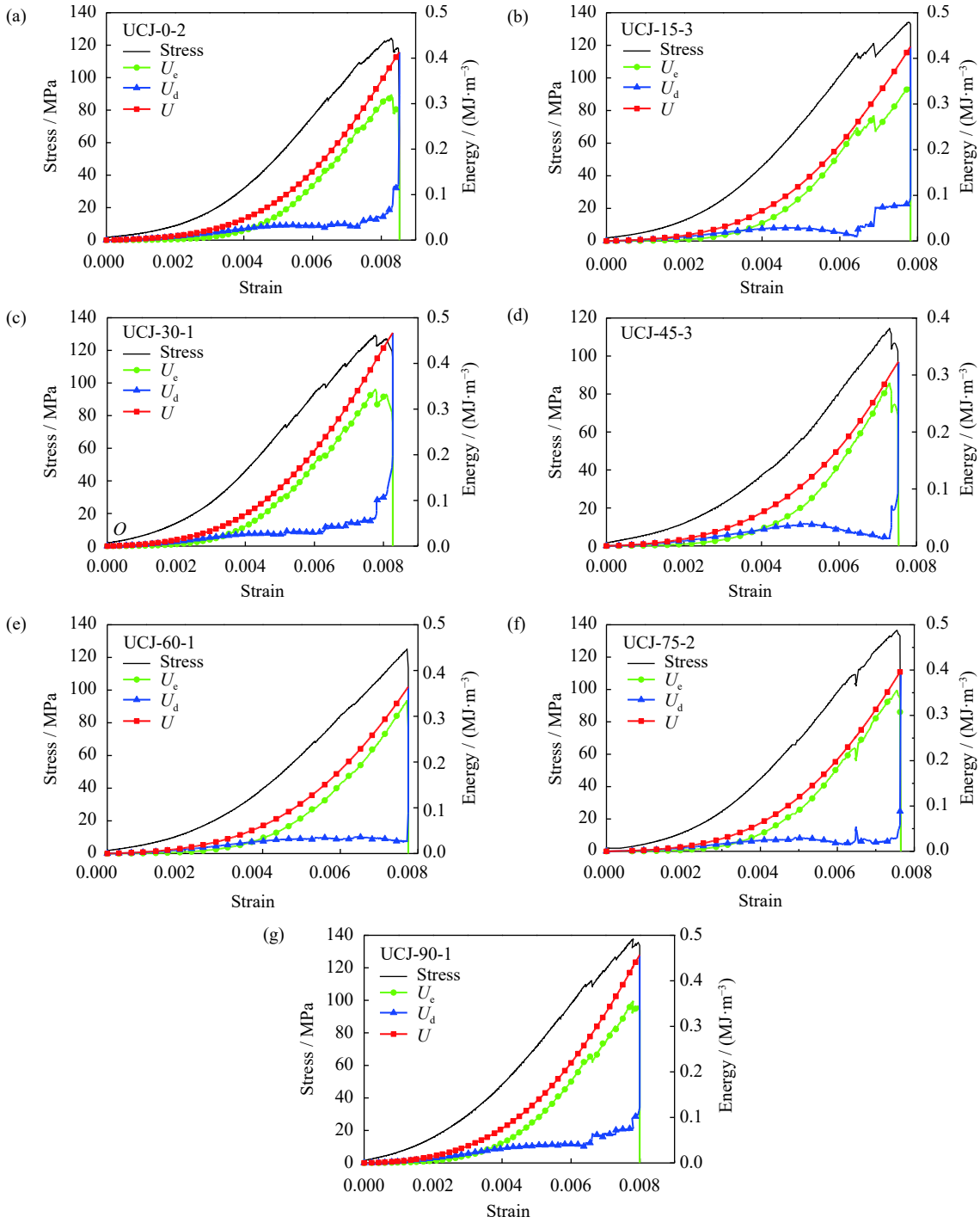

Fig. 8. Stress–strain and energy evolution curves of the parallel jointed samples containing an opening: (a) α = 0°; (b) α = 15°; (c) α = 30°; (d) α = 45°; (e) α = 60°; (f) α = 75°; (g) α = 90°.

sample, relatively few cracks are formed at this stage. U and U_e values still show an approximately linear increase with strain, while U_d is basically unchanged. In the unstable crack propagation stage, U and U_e continually increase as the strain increases. However, the growth rate of U_e gradually slows down and its value is maximized until it reaches the peak point. The dissipated energy increases in a "step" shape from the steady state, and its growth rate gradually increases. This process is not obvious in UI, but it is more distinct in UC and UCJ. After the accumulated elastic strain energy reaches the energy storage limit, the residual strength is instantly released and transferred to dissipated energy, leading to the drastic increase of the dissipated energy, which is the energy source of the specimen failure.

As seen from Figs. 7–8, the evolution curves of the U_e and U_d with strain of UI are relatively smooth, while that of UC

and UCJ show step-like gradual mutation characteristics. This phenomenon suggests that the internal stress of UI is quite uniform in the process of deformation and failure. Moreover, the observed behavior implies that the local stress concentration does not occur and the cracks are uniformly distributed. The cracks suddenly penetrate to form a macroscopic rupture surface, resulting in the failure of specimens, which belongs to a typical damage cumulative induced mutation failure mode. However, the internal stress distribution of the UC and UCJ is uneven. Obvious stress concentration will be formed at the joint tips and around the opening, causing cracks to begin to initiate, expand, and coalesce, which finally leads to the overall failure of the specimens. This is a typical progressive damage and failure mode. Therefore, the characteristics of energy evolution provide a method to further understand the rock energy conversion mechanism.

Table 1 shows the total input energy of the three kinds of samples under uniaxial loading and the calculated values of the total energy, elastic strain energy, and dissipated energy when stress–strain curves reach the peak. The total input energy is observed to be the largest for UI (1.016 MJ/m^3), followed by UC (0.643 MJ/m^3), showing a decrease of 36.71%, and finally by UCJ with a total input energy value between 0.323 and 0.467 MJ/m^3, which is 54.04%–68.21% lower than that of UI. Consequently, the total input energy of UCJ is significantly less than that of UI, which indicates that the opening and joints in the sample greatly weaken the overall strength of the sample, thus reducing the energy consumption in the process of deformation and failure. The highest peak elastic strain energy is achieved by UI (0.912 MJ/m^3), followed by UC (0.526 MJ/m^3) with a reduction of 42.32%, and finally followed by UCJ with a peak elastic strain energy in the range of 0.286–0.356 MJ/m^3, which is 60.96%–68.64% lower than that of UI. The peak elastic strain energy can be used as the energy storage limit of the sample to reflect its ability to accumulate elastic deformation energy and resist damage, while the opening and joints seriously weaken the energy storage limit of the sample. UCJ with different inclination angles and stress states exhibit different energy storage limits. UI has the highest strength and the maximum energy storage limit, while the energy storage limits of UC and UCJ have declined to varying degrees compared to UI. In particular, the energy storage limits of UCJ are relatively small with an inclination angle of 45°. The smaller the energy storage limit of the sample, the more likely it is to be driven by energy and damage. In addition, compared with the intact rock mass, the jointed rock mass has far weaker energy storage and rapid energy release capacity. Because of this, rock bursts are more likely to occur during the excavation process of underground chambers in the intact hard rock mass. In turn, the result has led to the use of loosening blasting in the advanced borehole to create fractured zones in the intact rock mass, thus greatly reducing the probability and intensity of rock bursts in chambers.

Table 1. Energy values of the samples under uniaxial loading MJ/m^3

Specimen	Peak total energy	Peak elastic strain energy	Peak dissipated energy	Total input energy
UI-2	0.941	0.912	0.029	1.016
UC-3	0.632	0.526	0.106	0.643
UCJ-0-2	0.384	0.320	0.064	0.413
UCJ-15-3	0.419	0.337	0.082	0.426
UCJ-30-1	0.405	0.344	0.061	0.467
UCJ-45-3	0.298	0.286	0.012	0.323
UCJ-60-1	0.361	0.335	0.026	0.364
UCJ-75-2	0.385	0.356	0.029	0.397
UCJ-90-1	0.432	0.356	0.076	0.457

Fig. 9 presents the variation trends of the total energy, elastic strain energy, and dissipated energy at peak points and the total input energy of UCJ as a function of inclination angle. It can be seen that all four kinds of energy of UCJ showed an overall trend of decreasing at first and then increasing as the inclination angle increases, reaching the minimum values when $\alpha = 45°$. Therefore, the energy absorption and utilization efficiency of the jointed rock mass is closely correlated with the inclination angle, which will lead to different energy release characteristics when the jointed rock mass is damaged. The observation results can be applied to dynamic disasters (such as rock bursts, collapse, spalling, and roof fall) monitoring [18]. Moreover, the changing trend of energy has a good correspondence with the trends of strength and deformation parameters (Fig. 6) of UCJ, which appears to reflect the intrinsic connection between the energy properties and mechanical performance of rocks.

The above analysis indicates that elastic strain energy and dissipated energy jointly determine the failure process in the brittle granite. Even with similar lithology, the energy evolution of samples will still vary because of the existence of the opening and joints and the change of the inclination angle. Owing to the original damage resulting from the artificial opening and joints and the dissipated energy caused by the

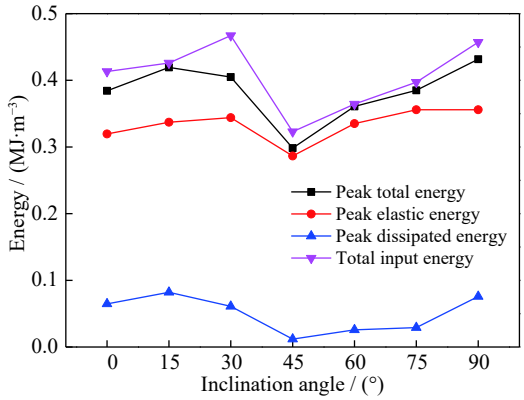

Fig. 9. Evolution of energy values of the parallel jointed samples containing an opening with the inclination angle.

crack initiation and propagation at the joint tips and near the opening in the process of deformation and failure, the energy absorption capacity of UCJ is greatly weakened. In other words, the opening and joints have a significant energy weakening effect on the granite.

4.2. Energy distribution law

For different types of specimens, the distribution proportions of the energy parameters will be different while converting external total energy input to the elastic strain energy and dissipated energy, which may affect the deformation and failure mode of the samples. Because the sum of the proportions of the elastic strain energy and dissipated energy to the total input energy equates 100%, only the curves of the elastic strain energy proportion versus strain for the samples during the process of deformation and failure are given (Fig. 10), which reflects the joint effect of the energy distribution law of the samples.

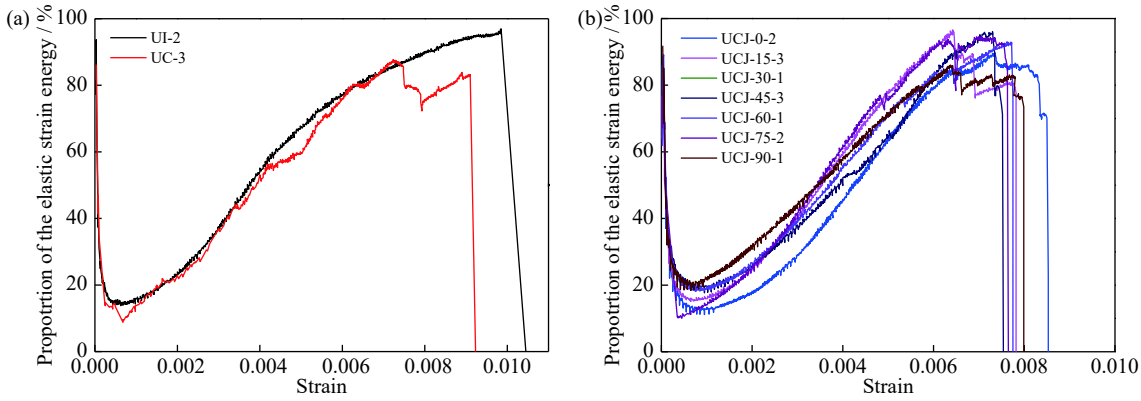

Fig. 10. Variation of the proportion of the elastic strain energy with strain of the samples: (a) the intact sample and the intact sample containing an opening; (b) the parallel jointed samples containing an opening.

In general, the energy distribution modes of all samples are similar. The proportion of the elastic strain energy is generally higher than that of the dissipated energy prior to the peak point, i.e., the energy input into the samples is mostly stored as elastic strain energy. Nevertheless, there are also cases where the proportion of the elastic strain energy is less than or similar to that of the dissipated energy. The opening and joints have little influence on the energy distribution proportion, which indicates that all samples have similar energy transformation laws in the pre-peak loading process and are dominated by energy accumulation. Specifically, as the specimen is subject to loading, the proportion of elastic strain energy is close to 100%, which is caused by the adjustment of the specimen to the load. At this time, the stress level is not enough to close the original microcracks, and energy dissipation does not appear. The proportion of elastic strain energy is relatively small at the initial compaction stage and gradually increases after the specimen enters the elastic deformation stage. Due to the brittle characteristics of the granite, the proportion of the elastic strain energy suddenly decreases when the specimen is near failure. Moreover, the proportion of the dissipated energy has an opposite change trend with the elastic strain energy, and the proportion of dissipated energy is larger due to the closure and friction of the original microcracks at the primary compaction stage. However, as load increases, the proportion of the dissipated energy gradually stabilizes at a lower level, and suddenly increases because of the propagation and coalescence of macrocracks.

The minimum elastic strain energy proportions of UI and UC at the initial compaction stage are 13.79% and 8.81%, respectively, and the maximum elastic strain energy proportions at peak strength are 96.97% and 83.21%, respectively (Fig. 10(a)). The minimum elastic strain energy proportions of UCJ with inclination angles of 0°–90° in the initial compaction stage are between 10.03% and 18.43%, and the maximum elastic strain energy proportions at peak strength are in the range of 80.42% and 96.05% (Fig. 10(b)). It can be seen that the opening and joints and the change of inclination angle have great influences on the proportion of the elastic strain energy prior to the peak point. Moreover, some differ-

ences are observed in the distribution law of the input energy. Before reaching the peak, the curve of the elastic strain energy proportion versus strain of UI grows smoothly, and there is almost no sudden change in the dissipated energy. However, the curves of the elastic strain energy proportion versus strain of UCJ fluctuate in different degrees, which corresponds to the stress characteristics of the samples, reflecting the influence of the opening and joints on the energy storage of the samples in the process of deformation and failure. The energy accumulation efficiency of UC and UCJ is not as good as that of UI. When UC and UCJ approach failure, the main cracks will propagate along with the joint tips and around the opening, and the elastic strain energy will be released in quantity. The fractured rock blocks will slip and rub along the main cracks, the dissipated energy will increase, and the axial strain and lateral strain will increase significantly [19]. After the fractured structure of the sample is reconstructed and stabilized, the sample reaches the residual strength and still has a certain energy accumulation ability. However, the energy accumulation efficiency is remarkably lower than that before the peak point.

4.3. Energy mechanism of the sample failure

The energy dissipation of specimens caused damage to the internal structure of the samples, leading to a gradual decline of the bearing capacity of the sample to ultimate instability and failure. It can be seen that the specimen instability and failure are closely related to its internal energy dissipation, and thus, can represent the damage degree of the samples. Taking the sample UCJ-30-1 for example, on the basis of the evolution law of the dissipated energy of UCJ, the sample damage and failure process roughly consists of four stages, namely, initial damage stage, stable damage stage, unstable damage stage, and unstable failure stage (Fig. 11).

(1) Initial damage stage (I). A small amount of energy dissipation occurs during the compaction process of the original microcracks, and the dissipated energy has a slight increase as load increases. However, the overall damage degree of the specimen is low. Moreover, one part of the energy input from external force gets lost as dissipated energy, while the remaining energy is preserved in the specimen as elastic strain energy. In general, the dissipated energy at this stage surmounts the accumulated elastic strain energy.

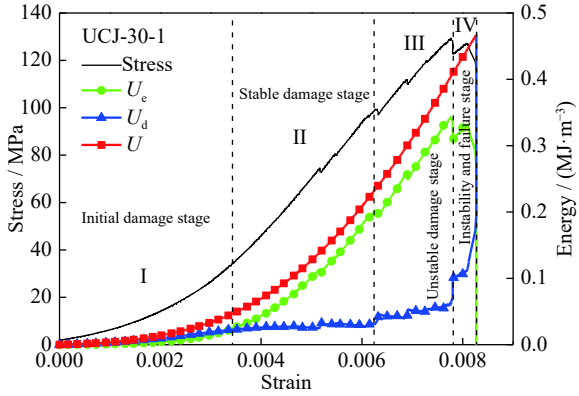

Fig. 11. Segmentation of energy evolution of the parallel jointed samples containing an opening.

(2) Stable damage stage (II). After the original microcracks are almost compressed, the specimen enters the stable damage stage. The dissipated energy evolves approximately horizontally with increasing load and the dissipated energy is small, indicating that the damage degree in the specimen is still relatively low. However, the elastic strain energy increases linearly as the load increases and the total input energy from the external force is mostly transformed to elastic strain energy and preserved in the specimen. This stage is the main energy storage stage of the sample.

(3) Unstable damage stage (III). When the load increases to a certain extent, the stress concentration formed around the opening and joint tips becomes prominent, which will result in the initiation and propagation of cracks. The damage of the sample begins to develop rapidly in this stage. Furthermore, the curve of the elastic strain energy accumulated in the specimen deviates from the total energy curve and drops steeply. Accordingly, the dissipated energy curve changes abruptly from the approximate horizontal evolution to a sudden increase in the "step" shape. The damage inside the specimen develops unsteadily, and cracks may appear intensively.

(4) Instability and failure stage (IV). As the bearing capacity of the sample reaches its peak strength, the sample begins to enter the instability and failure stage. The elastic strain energy stored in the specimen will be released quickly, the cracks further expand and penetrate to form macroscopic fracture surfaces, and the strength failure occurs, showing obvious brittleness characteristics. The dissipated energy increases suddenly and sharply, the elastic strain energy drops rapidly to nearly zero, and the elastic strain energy curve and the dissipated energy curve basically coincide.

The above-identified stages can well reveal the damage evolution feature of UCJ during deformation and failure. Essentially, the instability and failure of rock mass in underground engineering are induced by the driving action of energy. The evolution process of energy accumulation and dissipation in the rock mass is closely correlated with the gestation process of engineering disasters. The relative proportion of energy accumulation and dissipation directly determines the intensity and level of destruction of the engineering disasters. If a rock mass is prone to accumulate high elastic strain energy and has a strong energy release capacity, the possibility and intensity of induced engineering disasters will be greatly increased.

The rock deformation and failure process is complicated, from local damage to partial failure and final catastrophic instability, with significant nonlinear characteristics (Fig. 12).

In addition, for rock mass under any stress state, there is a limit value of energy storage. Once this limit value is reached, rock mass becomes unstable and destroyed. In other words, the deformation and failure process of rocks proceeds with energy input, accumulation, and dissipation. This signifies that energy plays a fundamental role in this process. Therefore, from the perspective of energy, three characteristic conditions are probably required for the dynamic failure of brittle rock mass in engineering [20]: (1) there is a good deal of elastic strain energy preserved in rock mass; (2) the rock mass reaches its energy storage limit; and (3) the energy release must be sharp and massive during rock mass failure. Energy dissipation induces damages to rock mass and triggers local degradation and strength loss, while the energy release can be considered as the internal cause of the sudden destruction to the whole rock mass. Therefore, rock mass failure is a necessary consequence of the sudden release of energy in the rock mass, which is a sudden change of energy dissipation under certain conditions [3,21].

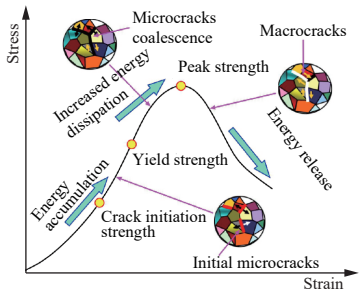

Fig. 12. Illustration of the link between rock deformation and failure process and energy evolution.

In engineering practice, the stress path of rock mass from one stress state to another is often very complicated. Rock masses with different initial stress states experience different stress paths when they reach the same energy state. When the slope of the energy path from the initial stress state to the energy storage limit state is large, the rock mass has approached the critical level in the high energy storage condition [20]. In this case, the rock mass can easily release strong energy under engineering disturbance or external disturbance, which consequently results in dynamic disaster. Therefore, the key to disaster prevention and control in rock engineering is to avoid the formation of high stress (energy) concentration in the surrounding rock of key parts of the project [22–24]. On the other hand, fracture development areas often refer to areas where joints are developed and the hydraulic conductivity of rock mass is enhanced. Joints in the surrounding rock have a strong induction effect on chamber instability, and the opening of rock joints may increase the inflow of water, thus affecting the long-term and short-term stability of caverns [19,25]. Because the energy storage limit of jointed rock mass is far less than that of intact rock mass, and thus, immediate supports, such as anchor cables, rockbolts, and shotcrete, in fracture development areas are required.

5. Conclusions

(1) The stress–strain curve of the parallel jointed samples with an opening generally consists of five stages: (1) initial compaction stage, (2) elastic deformation stage, (3) stable crack propagation stage, (4) unstable crack propagation stage, and (5) residual strength stage. The strength and deformation parameters of the parallel jointed samples with an opening decrease as the inclination angle increases from 0° to 45°, and increase as the inclination angle increases from 45° to 90°, reaching the minimum and maximum values when the inclination angles are 45° and 90°, respectively. Significant nonlinear characteristics are exhibited.

(2) The total energy and elastic strain energy show a nonlinear growth trend as the load increases. The elastic strain energy grows first and then decreases. However, the dissipated energy increases very slowly before the specimen failure and suddenly exceeds the elastic strain energy as the sample approaches failure. The evolution curves of the elastic strain energy and dissipated energy with strain of the intact sample are relatively smooth, and the evolution curves of the two types of energy with strain of the intact sample containing an opening and the parallel jointed samples containing an opening show step-like gradual mutation characteristics.

(3) The opening and joints in the sample weaken the overall strength and reduce the energy consumption during the failure of the sample. The peak total energy, peak elastic strain energy, peak dissipated energy, and the total input energy of the parallel jointed samples containing an opening first decreased and then increased as the inclination angle increases, with the smallest values achieved at the inclination angle of 45°.

(4) The opening and joints have a significant energy weakening effect on the samples. Moreover, the opening and joints with different inclination angles have great influences on the proportion of the elastic strain energy of the samples before the peak point, resulting in the difference in the distribution law of input energy. In addition, energy dissipation damages rock mass and triggers local degradation and strength loss. The energy release is considered as the internal cause of the sudden destruction of the whole rock mass.

Acknowledgements

This work was financially supported by the Interdisciplinary Research Project for Young Teachers of USTB (Fundamental Research Funds for the Central Universities) (No. FRF-IDRY-20-013), the National Natural Science Foundation of China (Nos. 51774022, 52074020, and 51604017), the State Key Research Development Program of China

(Nos. 2016YFC0600801 and 2017YFC0804103), and the Youth Fund Project of Education Department of Hebei Province, China (No. QN2018202).

References

[1] M.Q. You and A.Z. Hua, Energy analysis on failure process of rock specimen, *Chin. J. Rock Mech. Eng.*, 21(2002), No. 6, p. 778.

[2] H.P. Xie, R.D. Peng, and Y. Ju, Energy dissipation of rock deformation and fracture, *Chin. J. Rock Mech. Eng.*, 23(2004), No. 21, p. 3565.

[3] H.P. Xie, R.D. Peng, Y. Ju, and H.W. Zhou, On energy analysis of rock failure, *Chin. J. Rock Mech. Eng.*, 24(2005), No. 15, p. 2603.

[4] Z.Z. Zhang and F. Gao, Research on nonlinear characteristics of rock energy evolution under uniaxial compression, *Chin. J. Rock Mech. Eng.*, 31(2012), No. 6, p. 1198.

[5] J.P. Zuo, Y.M. Huang, G.J. Xiong, J. Liu, and M.M. Li, Study of energy-drop coefficient of brittle rock failure, *Rock Soil Mech.*, 35(2014), No. 2, p. 321.

[6] Z.Y. Li, G. Wu, T.Z. Huang, and Y. Liu, Variation of energy and criteria for strength failure of shale under traixial cyclic loading, *Chin. J. Rock Mech. Eng.*, 37(2018), No. 3, p. 662.

[7] F.Q. Gong, S. Luo, X.B. Li, and J.Y. Yan, Linear energy storage and dissipation rule of red sandstone materials during the tensile failure process, *Chin. J. Rock Mech. Eng.*, 37(2018), No. 2, p. 352.

[8] W.L. Liu, E.C. Yan, H. Dai, Y. Du, W.B. Xiao, and S. Zhao, Study on characteristic strength and energy evolution law of Badong formation mudstone under water effect, *Chin. J. Rock Mech. Eng.*, 39(2020), No. 2, p. 311.

[9] Q.B. Meng, C.K. Wang, B.X. Huang, H. Pu, Z.Z. Zhang, W. Sun, and J. Wang, Rock energy evolution and distribution law under triaxial cyclic loading and unloading conditions, *Chin. J. Rock Mech. Eng.*, 39(2020), No. 10, p. 2047.

[10] G.Q. Chen, J.C. Wu, W.Z. Jiang, S.J. Li, Z.B. Qiao, and W.B. Yang, An evaluation method of rock brittleness based on the whole process of elastic energy evolution, *Chin. J. Rock Mech. Eng.*, 39(2020), No. 5, p. 901.

[11] Z.T. Bieniawski and M.J. Bernede, Suggested methods for determining the uniaxial compressive strength and deformability of rock materials: Part 1. Suggested method for determining deformability of rock materials in uniaxial compression, *Int. J. Rock Mech. Min. Sci. Geomech. Abstr.*, 16(1979), No. 2, p. 138.

[12] L. Weng, X.B. Li, A. Taheri, Q.H. Wu, and X.F. Xie, Fracture evolution around a cavity in brittle rock under uniaxial compression and coupled static–dynamic loads, *Rock Mech. Rock Eng.*, 51(2018), No. 2, p. 531.

[13] X.G. Zhao, M. Cai, J. Wang, and L.K. Ma, Damage stress and acoustic emission characteristics of the Beishan granite, *Int. J. Rock Mech. Min. Sci.*, 64(2013), p. 258.

[14] V. Hajiabdolmajid, P.K. Kaiser, and C.D. Martin, Modelling brittle failure of rock, *Int. J. Rock Mech. Min. Sci.*, 39(2002), No. 6, p. 731.

[15] Z.L. Zhou, L.H. Tan, W.Z. Cao, Z.Y. Zhou, and X. Cai, Fracture evolution and failure behaviour of marble specimens containing rectangular cavities under uniaxial loading, *Eng. Fract. Mech.*, 184(2017), p. 183.

[16] P. Li, F.H. Ren, M.F. Cai, Q.F. Guo, H.F. Wang, and K. Liu, Investigating the mechanical and acoustic emission characteristics of brittle failure around a circular opening under uniaxial loading, *Int. J. Miner. Metall. Mater.*, 26(2019), No. 10, p. 1217.

[17] X.P. Zhou, J. Z. Zhang, Q.H. Qian, and Y. Niu, Experimental investigation of progressive cracking processes in granite under uniaxial loading using digital imaging and AE techniques, *J. Struct. Geol.*, 126(2019), p. 129.

[18] X.Q. He, C. Zhou, D.Z. Song, Z.L. Li, A.Y. Gao, S.Q. He, and M. Khan, Mechanism and monitoring and early warning technology for rockburst in coal mines, *Int. J. Miner. Metall. Mater.*, 28(2021), No. 7, p. 1097.

[19] P. Li and M.F. Cai, Energy evolution mechanism and failure criteria of jointed surrounding rock under uniaxial compression, *J. Cent. South Univ.*, 28(2021), No. 6, p. 1857.

[20] Z.Z. Zhang and F. Gao, Confining pressure effect on rock energy, *Chin. J. Rock Mech. Eng.*, 34(2015), No. 1, p. 1.

[21] H.P. Xie, Y. Ju, and L.Y. Li, Criteria for strength and structural failure of rocks based on energy dissipation and release principles, *Chin. J. Rock Mech. Eng.*, 24(2005), No. 17, p. 3003.

[22] P. Li, M.F. Cai, Q.F. Guo, and S.J. Miao, Characteristics and implications of stress state in a gold mine in Ludong area, China, *Int. J. Miner. Metall. Mater.*, 25(2018), No. 12, p. 1363.

[23] X.H. Wu, Q.F. Guo, P. Li, F.H. Ren, J. Zhang, and M.F. Cai, Investigating the effect of temperature changes on the physical field of surrounding rock in a deep gold mine, *Adv. Mater. Sci. Eng.*, 2021(2021), art. No. 8490864.

[24] P. Li, M.F. Cai, Q.F. Guo, and S.J. Miao, *In situ* stress state of the northwest region of the Jiaodong peninsula, China from overcoring stress measurements in three gold mines, *Rock Mech. Rock Eng.*, 52(2019), p. 4497.

[25] P. Li, Y.Q. Wu, and Y. Zhang, Mechanical and acoustic responses of brittle geomaterials with a hole under a compressive disturbance, *Adv. Mater. Sci. Eng.*, 2021(2021), art. No. 5292925.